HHS Public Access

Author manuscript

Cell Rep Phys Sci. Author manuscript; available in PMC 2025 March 13.

Published in final edited form as:

Cell Rep Phys Sci. 2025 February 19; 6(2): . doi:10.1016/j.xcrp.2025.102441.

Transporter excess and clustering facilitate adaptor protein shuttling for bacterial efflux

Wenyao Zhang[1,4,5,10], **Christine E. Harper**[2,3,6,10], **Junsung Lee**[2,3], **Bing Fu**[1,7], **Malissa Ramsukh**[2,8], **Christopher J. Hernandez**[2,9,*], **Peng Chen**[1,11,*]

[1]Department of Chemistry and Chemical Biology, Cornell University, Ithaca, NY 14853, USA

[2]Sibley School of Mechanical and Aerospace Engineering, Cornell University, Ithaca, NY 14853, USA

[3]Meinig School of Biomedical Engineering, Cornell University, Ithaca, NY 14853, USA

[4]Present address: US Military HIV Research Program, Walter Reed Army Institute of Research, Silver Spring, MD 20910, USA

[5]Present address: The Henry M. Jackson Foundation for the Advancement of Military Medicine, Bethesda, MD 20817, USA

[6]Present address: Chronus Health, 34175 Ardenwood Boulevard, Fremont, CA 94555, USA

[7]Present address: Department of Biomedical Engineering, City University of Hong Kong, Hong Kong 999077, China

[8]Present address: Department of Neuroscience, Albert Einstein College of Medicine, Bronx, NY 10461, USA

[9]Present address: Departments of Bioengineering and Therapeutic Sciences and Orthopedic Surgery, University of California, San Francisco, San Francisco, CA 94143, USA

[10]Equal contributions

[11]Lead contact

SUMMARY

Multidrug efflux pumps confer not only antibiotic resistance to bacteria but also cell proliferation. In gram-negative bacteria, the ATP-binding cassette (ABC)-family transporter MacB, the adaptor

*Correspondence: christopher.hernandez@ucsf.edu (C.J.H.), pc252@cornell.edu (P.C.).

AUTHOR CONTRIBUTIONS

W.Z. designed experiments, constructed strains, performed all imaging and biochemical experiments, analyzed data, and wrote the manuscript. C.E.H. fabricated microfluidic devices, performed mechanical loading experiments, analyzed data, and wrote the manuscript. J.L. performed finite element modeling. B.F. contributed to strain construction. M.R. contributed to image processing. C.J.H. directed mechanical manipulation research and wrote the manuscript. P.C. directed biological and imaging research and wrote the manuscript.

DECLARATION OF INTERESTS

The authors declare no competing interests.

SUPPLEMENTAL INFORMATION

Supplemental information can be found online at https://doi.org/10.1016/j.xcrp.2025.102441.

protein MacA, and the outer membrane protein TolC form the $MacA_6$:$MacB_2$:$TolC_3$ assembly to extrude antibiotics and virulence factors. Here, using quantitative single-molecule single-cell imaging, we uncover that, in *E. coli* cells, there is a large excess of MacB (and TolC) driving the limiting adaptor protein MacA mostly into the MacAB-TolC assembly. Moreover, the excess MacB transporters can dynamically cluster around the assembly, and MacA can dynamically disassemble from the MacAB-TolC assembly, leading to an adaptor protein shuttling mechanism for efficient substrate sequestration from the periplasm toward efflux. We further show that both MacB clustering and MacAB-TolC assembly can be perturbed chemically or physically via microfluidics-based extrusion loading for compromised antibiotic tolerance. These insights may provide opportunities for countering the activities of multidrug efflux systems for antimicrobial treatments.

In brief

Multidrug efflux pumps (MEPs) serve vital roles in bacterial survival by expelling antibiotics and other physiological substrates from the cell. Here, Zhang et al. uncover an adaptor protein shuttling mechanism of MacAB-TolC, an unconventional MEP of the ABC family, improving the understanding of protein interactions and providing new perspectives for antimicrobial treatments.

Graphical Abstract

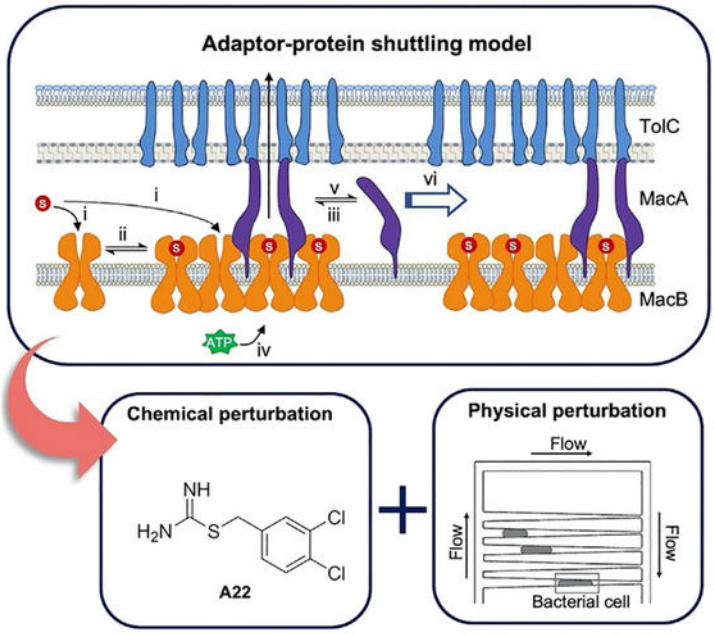

INTRODUCTION

Bacterial infection is a major public health issue. The development of antibiotic resistance makes treatment increasingly challenging, especially for gram-negative bacteria, which are insensitive to a wide range of antibiotics due to the additional outer membrane (OM).[1,2] For pathogenic bacteria, virulence and antibiotic resistance are two sides of the same coin to overcome adverse conditions in the host.[3] Multidrug efflux pumps, which constitute a ubiquitous and highly conserved resistance mechanism, not only can actively extrude a large variety of antimicrobial agents but are also involved in the export of virulence factors.[4–6]

In gram-negative bacteria, multidrug efflux pumps are categorized based on the inner membrane (IM) transporter.[5–7] Transporters in the ATP-binding cassette (ABC) superfamily, the largest superfamily present in all organisms, are energized by ATP hydrolysis. These transporters usually form tripartite complexes with a periplasmic adaptor protein and an OM pore protein, traversing the cell envelope and extruding substrates into the extracellular environment.[6] MacB, an essential ABC-superfamily transporter in many gram-negative bacteria, including *Escherichia coli*, forms the MacAB-TolC complex with the periplasmic adaptor protein MacA (which is anchored on the IM via an N-terminal helix[8,9]) and the OM channel protein TolC (a promiscuous OM protein in huge abundance in the cell) with A_6:B_2:C_3 stoichiometry (Figure 1A, left).[10–12] Many biophysical, biochemical, and genetic studies have provided insights into the structure and function of the MacAB-TolC complex.[13] MacAB-TolC confers resistance to diverse antibiotics, including macrolide drugs, bacitracin, and colistin; moreover, it secretes endogenous substrates related to virulence factor and heme hemostasis (e.g., enterotoxin STII, lipopolysaccharide, and protoporphyrin IX) (Figure 1A, right).[9,10,14–16] The MacB homodimer has a nucleotide-free (open) and an ATP-bound (closed) form; both forms lack a transmembrane cavity (an unconventional feature for ABC transporters), indicating that MacB captures substrates directly from the periplasm.[10] In the assembled complex, besides connecting MacB and TolC, the hexameric MacA stimulates MacB's ATPase activity,[12,17] and ATP binding to the MacB dimer induces a more compact structure via conformational changes of its transmembrane and periplasmic domains in a so-called mechano-transmission mechanism, pumping out the substrate.[10]

Many aspects remain unclear about the functional mechanism of MacAB-TolC, however. First, it is unclear whether the cellular levels of the three proteins follow the 6:2:3 stoichiometry as in the assembled complex. The promiscuous OM channel protein TolC is in large abundance (~1,500 copies in *E. coli*[18]), and, thus, is likely in large excess. Second, although a possible portal for substrate entry has been proposed based on the crystal structure of the MacB dimer, such a portal is likely less accessible in the assembled MacAB-TolC.[12] Third, there is no discernible substrate-induced conformational change in MacB, and MacA likely forms a complex with MacB with or without substrate; the latter would be unproductive for the usage of ATP. Previous studies have shown that tripartite efflux complexes can undergo dynamic assembly in response to substrates.[19,20] This dynamic assembly would, in principle, solve the substrate entry problem of MacAB-TolC, but whether it is applicable here is unknown, and little is known concerning the dynamics of the MacAB-TolC complex in cells.[21,22]

Here, we use single-molecule single-cell fluorescence microscopy to quantify the spatial and temporal behaviors of MacAB-TolC in live *E. coli* cells. We find that the cellular concentrations of the three proteins do not follow their designated assembly stoichiometry but instead have a large excess of MacB (and TolC) to drive the limiting adaptor protein MacA mostly into the MacAB-TolC assembly. The excess MacB transporters can dynamically cluster around the assembly, and MacA can dynamically disassemble from the complex, leading to an adaptor protein shuttling mechanism for efficient substrate sequestration from the periplasm toward efflux. Moreover, both MacB clustering and MacAB-TolC assembly can be perturbed chemically and physically for compromised antibiotic tolerance. Taken together, our findings reveal a distinct efflux mechanism for the multidrug efflux pump in gram-negative bacteria and can help with the development of antimicrobial treatments.

RESULTS

Single-cell protein quantitation identifies an excess of cellular MacB

First, we checked whether the cellular proteins follow the MacA:MacB:TolC = 6:2:3 stoichiometry as in the assembled MacAB-TolC complex under physiological conditions. TolC is known to have ~1,500 copies in *E. coli*.[18] To quantify cellular MacB or MacA encoded in the *macAB* operon,[16] we tagged them with fluorescent protein fusions at their chromosomal loci (Note S1; Tables S1–S3). The IM transporter MacB was tagged at its cytosol-exposed C terminus with the photoconvertible mEos3.2 (i.e., $MacB^{mE}$).[23] The adaptor protein MacA was tagged at its periplasm-exposed C terminus with the photoactivatable PAmCherry1 (i.e., $MacA^{PmC}$),[24] which does not contain cysteine residues and can mature properly in the periplasm.[25,26] Both mEos3.2 and PAmCherry1 allow controlled photoconversion/photoactivation and subsequent single-molecule imaging, tracking, and counting. Tagging either MacB or MacA retained the efflux function of MacAB-TolC against macrolides (Figures S1A and S1B), whereas the strain in which both proteins were tagged could not be shown reliably to be functional in macrolide efflux and was thus not studied further (Figure S1C). Upon overexpression to facilitate imaging sensitivity in conventional confocal microscopy, both $MacB^{mE}$ and $MacA^{PmC}$ appeared to be localized on the cell envelope as expected (Figure 1B). Moreover, immunoblotting showed that the $MacB^{mE}$ fusion is intact and that $MacA^{PmC}$ has less than ~30% of cleavage even under overexpression (Figure S2), further supporting the conclusion that they are functional and mostly intact in the cell. The cleaved $MacA^{PmC}$ C-terminal fragment, which would be much less significant in the context of our single-molecule imaging experiments under physiological expression, should be nonfluorescent, as discussed below and expected from the literature.[27–29]

We measured the copy numbers of $MacB^{mE}$ and $MacA^{PmC}$ in individual cells using both single-molecule counting and whole-cell fluorescence quantitation (Note S1). These two methods yielded copy numbers of MacB and MacA at 60 ± 25 per cell on average (Figure 1C; the ± range here is the standard deviation among individual cells; note that 1 copy corresponds to ~1 nM in an *E. coli* cell). Even when considering potential $MacA^{PmC}$ cleavage, MacA is still less than ~85 copies, giving a cellular MacA:MacB molar ratio

of <1.5:1, about half of their 6:2 assembly stoichiometry and indicating the large cellular excess of the MacB transporter. The proteins' copy numbers do not change much when the other protein is deleted or when the cell is stressed with the efflux substrate erythromycin (Figures 1C, S4, and S5). The copy number quantitation is also independent of the fluorescent protein tag (i.e., mE vs. PmC; Figure S3). Together with the abundance of TolC, these cellular protein levels make MacA the limiting reagent in MacAB-TolC complex formation. Considering the interaction affinity of MacA-MacB being ~50 nM[22] and that of MacA-TolC being ~200 nM,[21] MacA should predominantly exist in the assembled MacAB-TolC complex, and free disassembled MacA should be a minor species in the cell.

Single-molecule tracking reveals dynamic MacAB-TolC interactions

Tagging with photoconvertible/activatable fluorescent proteins also allowed for single-molecule photo-conversion/activation and subsequent tracking at tens of nanometer spatial precision to quantify protein diffusion in the cell (Figure 2A, inset; Note S1).[19,30,31] The experimental distribution of displacement length r from the tracking trajectories is distorted by the cell confinement effect and 2D imaging projection, which can be deconvoluted by ITCDD (inverse transformation of confined displacement distribution) for both membrane[19,30,32] and cytosolic proteins[30,33] (Figure 2A; Note S4; Figures S6–S9).

For $MacB^{mE}$ in wild-type (WT) cells, the ITCDD-corrected displacement length distribution resolves two diffusion states (Figure 2A). One mobile state with a diffusion coefficient D_m of 0.83 ± 0.05 $\mu m^2 \cdot s^{-1}$ amounts to a population fraction of 27% ± 5% (A_m); this state is attributable to freely moving $MacB^{mE}$ dimers (Figure 4A), whose D_m is consistent with typical IM mobile proteins.[19,30] The other state (D_s = 0.055 ± 0.002 $\mu m^2 \cdot s^{-1}$) is quasi-stationary considering our tracking uncertainties and accounts for the dominant fraction of 73% ± 5% (A_s). A significant component of this quasi-stationary fraction should be the assembled $MacA_6B_2$-$TolC_3$ complex, whose linkage across the cell envelope should severely limit its mobility (Figure 1A). However, the assembled $MacA_6B_2$-$TolC_3$ complex cannot fully account for this quasi-stationary state of MacB, as the cellular MacB copies are twice as many as MacA (Figure 1C). We attribute the rest of this stationary state to clustered $MacB^{mE}$ dimers (i.e., $[MacB_2]_n$) that are either directly clustered with themselves or indirectly associated with other proteins (Figure 4B); such clustering is known to limit membrane protein diffusivity.[30,34] On a related note, the assembled $MacA_6B_2$-$TolC_3$ complex could also be among clustered MacB dimers (Figure 4B). Upon deleting both *macA* and *tolC* from the cell (i.e., ΔAC), MacAB-TolC complex formation is not possible, but the quasi-stationary state of $MacB^{mE}$ is still dominant at ~75% fraction (Figure 2B, column 4), further supporting the scenario of $MacB^{mE}$ clustering as a significant contributor here.

We also examined the ΔA single-deletion strain, in which $MacB^{mE}$ coexists with TolC on the IM and OM, respectively. Past studies have shown that MacB and TolC have weak to negligible interactions *in vitro*.[21,35] *E. coli*'s periplasmic space is ~17–35 nm thick,[36,37] while the periplasmic portions of MacB and TolC add up to only ~15 nm in dimension,[12,38] making their interactions even less possible. Therefore, $MacB^{mE}$ mobility in the ΔA strain should be like that in the ΔAC strain. Indeed, the same mobile and quasi-stationary diffusion

states are observed with comparable fractional populations (Figure 2B, column 2 vs. 4), which are dominated by free $MacB^{mE}$ dimers and their clusters, respectively. Additionally, in the ΔC single-deletion strain, $MacB^{mE}$ coexists with MacA but in excess relative to their 2:6 complex stoichiometry. MacA is known to form a tight complex with MacB.[22] Thus, in the absence of TolC, MacA is expected to bind and form some complex with both mobile and stationary fractions of $MacB^{mE}$, but this $MacB^{mE}$-MacA complex does not traverse the periplasm and may not substantially alter $MacB^{mE}$'s mobility. Experimentally, the same two diffusion states of $MacB^{mE}$ are observed in the ΔC strain with similar fractional populations as in the ΔAC strain (Figure 2B, column 3 vs. 4), supporting that MacA binding to MacB alone has no significant effect on $MacB^{mE}$ mobility.

Moreover, single-molecule tracking (SMT) directly gives displacement length r vs. time t trajectories for individual $MacB^{mE}$, in which r transitions between small and large values, reflecting dynamic interconversions between the quasi-stationary and mobile states (Figure S10). By analyzing such trajectories (Note S4), we can estimate the interconversion kinetics between $MacB^{mE}$'s two diffusion states.[30] In WT cells, $MacB^{mE}$'s interconversions are a convolution of assembly/disassembly for forming the MacAB-TolC complex and of clustering/declustering of MacB in the IM, and the effective rate constants are $k_{m\to s}$ = 14 ± 8 and $k_{s\to m}$ = 5 ± 3 s^{-1} (Figure 2D). On the other hand, in the ΔAC and ΔA strains, the interconversion kinetics dominantly report MacB's clustering/declustering; this interconversion is also on the order of 10^0 s^{-1} (Figure 2D), reflecting the dynamic nature of MacB's (de)clustering at the sub-second timescale (Figure 4, step ii).

In parallel, we used SMT to quantify $MacA^{PmC}$ diffusion in the cell. In the WT strain, two states are resolved (Figure 2C, column 1) with D values of 0.95 ± 0.08 $\mu m^2 \cdot s^{-1}$ for the mobile state and 0.062 ± 0.003 $\mu m^2 \cdot s^{-1}$ for the quasi-stationary state (Table S6). Importantly, no state was resolvable with D values close to those of cytosolic free diffusing proteins (~7 $\mu m^2 \cdot s^{-1}$)[39] or free periplasmic proteins (~3 $\mu m^2 \cdot s^{-1}$)[40,41] (Note S4); therefore, the cleaved tag of $MacA^{PmC}$ (<30% if under overexpression) is likely non-fluorescent and non-observable here, or the cleavage under physiological expression is negligible. Between the two resolved states, the quasi-stationary state of $MacA^{PmC}$ dominates (>65% of population), consistent with MacA being the limiting protein stoichiometrically for the MacAB-TolC complex and should exist dominantly in the assembled, quasi-stationary complex (Figure 4D). The other minor mobile population (<35%) could have contributions from either the moving unassembled $MacA^{PmC}$ (Figure 4C) or $MacA^{PmC}$ in complex with mobile MacB dimers. The latter is less likely, however, because its D_m value (~0.95 $\mu m^2 \cdot s^{-1}$) is slightly larger than that (~0.83 $\mu m^2 \cdot s^{-1}$) of the mobile $MacB^{mE}$ in the same WT strain (Tables S5 and S6), while MacA binding should only slow down MacB. Consequently, $MacA^{PmC}$'s interconversion between the two diffusion states here should dominantly reflect its dynamic assembly/disassembly regarding the MacAB-TolC complex, whose effective rate constants are approximately 7 ± 3 and 4 ± 1 s^{-1} (Figures 2E and 4, steps iii and v).

In the ΔB strain, where TolC is in large excess, $MacA^{PmC}$ should dominantly exist in the MacA-TolC complex that traverses the cell envelope, consistent with its stationary fractional population of >70% (Figure 2C, column 2). The mobile state (<30%) can only be unassembled $MacA^{PmC}$ here. Here, $MacA^{PmC}$'s interconversion between two diffusion

states reflects the dynamic MacA-TolC interactions at a rate of 10^0 s^{-1} (Figures 2E and 4, steps iii and v). In the ΔC strain, most $MacA^{PmC}$ should be complexed with MacB, as there is excess MacB in the cell. As a significant portion of MacB is in the clustered form, we assigned the dominant stationary fraction of $MacA^{PmC}$ here to its association with $[MacB_2]_n$ (Figure 2C, column 3). The interconversion kinetics should thus reflect the dynamic interactions between MacA and $[MacB_2]_n$ at a rate of 10^0 s^{-1} (Figures 2E and 4, steps iii and v). Interestingly, in the double-deletion ΔBC strain, we still observed ~60% of quasistationary $MacA^{PmC}$ (Figure 2C, column 4). This stationary fraction can only be explained by direct or indirect clustering of $MacA^{PmC}$ or by interaction with some other unidentified proteins, and this interconversion is dynamic as well (Figure 2E).

A parallel analysis of diffusion states and the inter-state transition kinetics of $MacB^{mE}$ and $MacA^{PmC}$ was also performed using variational Bayes single-particle tracking,[42] showing consistent results to support our analyses above (Note S4; Tables S7 and S8). Altogether, SMT of $MacB^{mE}$ and $MacA^{PmC}$ in cells supports that the MacAB-TolC complex is dynamic both in terms of the assembly of the three components and in terms of the direct or indirect clustering.

MacB and MacA show distinct spatial localizations in the cell

These diffusive behaviors suggest that MacB (and maybe MacA) proteins may cluster together directly or indirectly via interactions with other cellular components, which contributes to their respective quasi-stationary fractions. We therefore examined whole-cell wide-field fluorescence images (with a diffractionlimited resolution of ~300 nm), in which we photoconverted/activated all cellular $MacB^{mE}$ or $MacA^{PmC}$. $MacB^{mE}$ shows granular fluorescence patterns, supporting its clustering in the cell, while the spatial pattern of $MacA^{PmC}$ is somewhat diffuse (Figure 3A).

To further probe such clustering beyond diffraction-limited resolution, we analyzed the pairwise distance distributions (PWDD) from the first localizations of SMT trajectories (Note S5).[19,30] For $MacB^{mE}$ in the WT strain, its PWDD shows a clear peak at the short distance of ~80 nm, supporting its clustering (Figure 3B, black curve). We further separated the $MacB^{mE}$ localizations into two groups: those dominated by mobile dimers (Figure 3B, red) and those dominated by quasi-stationary molecules, which comprise the clustered form and the assembled MacAB-TolC complex (Figure 3B, blue). The PWDD for the mobile group has no discernible peak at short distances, as expected, while that for the quasi-stationary group shows a pronounced peak at ~80 nm. Moreover, such a peak does not appear in the PWDD of simulated localizations of dimeric proteins that are spatially distributed homogeneously on the cell surface (Figure 3B dashed line; Note S5), supporting the theory that this PWDD peak comes more from $MacB^{mE}$ clustering (Figure 4B) than from its being a dimeric protein (Figure 4A). Consistent with our earlier results showing that the quasi-stationary state is dominated by protein clustering, the PWDD peak at ~80 nm is observed across other $MacB^{mE}$-related strains (i.e., ΔA, ΔC, and ΔAC; Figure S11). Interestingly, across all strains, this PWDD peak has comparable fractional areas (Figure 3D), suggesting that, in the WT strain, the fully assembled MacAB-TolC is also part of the clustered $MacB^{mE}$ (Figure 4B).

Such a PWDD peak at the short distance of ~80 nm is also observed in all $MacA^{PmC}$ relevant strains (Figures 3C and S12), and in analogy to our discussion about $MacB^{mE}$, this peak is primarily contributed by $MacA^{PmC}$'s quasi-stationary state. However, its fractional area varies across these strains; the simulation of spatially homogeneous hexametric proteins shows a peak comparable to those of the WT and the ΔBC strain, which are significantly higher than those of the ΔB and ΔC strains (Figure 3D). In the absence of MacB or TolC, the quasi-stationary state of $MacA^{PmC}$ mainly consists of MacA-TolC complexes or $MacA^{PmC}$ complexed with clustered MacB, respectively. Considering both the PWDDs and the earlier state assignments, we conclude that, in the ΔB and ΔC strains, there is minimal $MacA^{PmC}$ clustering and that the inter-distances between $MacA^{PmC}$ molecules are diluted by MacA's nanomolar high-affinity interactions[21,22] with excess TolC or MacB without even forming hexamers. For the WT strain, the PWDD peak at ~80 nm likely comes predominantly from $MacA^{PmC}$ hexamerization in the fully assembled $MacA_6B_2$-$TolC_3$ complex (Figure 4D). In the ΔBC strain, $MacA^{PmC}$ is on its own at ~100 nM cellular concentration and hexamerizes, consistent with previous *in vitro* studies showing that MacA alone could hexamerize at high concentrations.[8]

Altogether, our PWDD analyses here support the existence of MacB clusters around the MacAB-TolC assembly, consistent with its cellular excess relative to MacA. The analyses further support that, in the WT strain, MacA, the stoichiometrically limiting component, is dominantly in the hexameric assembled form, ensuring its maximum usage for efflux.

Adaptor-protein shuttling model for MacAB-TolC function

Collectively, due to the large excess of the IM transporter MacB and OM channel TolC, the adaptor protein MacA predominantly exists in the $MacA_6B_2$-$TolC_3$ assembly in WT *E. coli* cells, which can dynamically disassemble at the sub-second timescale, while more than half of MacB is not in the MacAB-TolC assembly. Because of MacB's tendency to cluster, most assemblies are associated with clustered MacB, which can dynamically exchange with the mobile state at sub-second timescale. These stoichiometric, spatial, and temporal properties of the protein components led us to propose an adaptor protein shuttling model for MacAB-TolC's functional cycle (Figure 4): the excess freely moving MacB as well as the unassembled clustered MacB capture substrates from the periplasmic side (Figure 4A) (step i); the substrate-bound free MacB dynamically exchanges with the clustered MacB around the MacAB-TolC assembly (Figure 4B) (step ii); MacA shuttles over to form a complex with the substrate-bound MacB (step iii); the interaction with MacA activates MacB's ATP binding and hydrolysis, thereby extruding the substrate[10] (step iv); the complex disassembles after ATP hydrolysis (step v); and the disassembled MacA then shuttles to another nearby substrate-bound MacB for the next round of efflux, repeating step iii (Figure 4C).

This model is further supported by the literature and addresses prior knowledge gaps about MacAB-TolC function. For step i (Figure 4), unlike conventional ABC transporters, MacB lacks central cavities within its transmembrane domains for substrate translocation across the IM.[12,43,44] Instead, the periplasmic domains of MacB capture substrates that are transported into the periplasm by other machineries or enter the periplasm from the outside.

Previous structural studies did not uncover easily accessible pathways for physiological substrates to enter the assembled MacAB-TolC. Therefore, the excess vacant MacB, either freely moving or clustered, provides direct access for substrate binding (Figure 4A), efficiently scavenging and sequestering substrates from the periplasm, and as shown in step ii, the freely moving MacB can also dynamically form clusters close to the MacAB-TolC assembly (Figure 4B). Regarding steps iii and iv, the adaptor protein MacA caps over the substrate-bound MacB, increasing its affinity to ATP[35,45]; further complexing with TolC again increases ATP affinity[46] and forms a complete conduit to the extracellular environment (Figure 4D). Here, the excess MacB and TolC in the cell help drive the formation of the complete MacAB-TolC assembly to minimize the bipartite complex MacB-MacA, which could otherwise lead to ineffective ATP recruitment. The binding of ATP to MacB squeezes the substrate out of the periplasmic cavity via mechano-transmission,[10] and the following ATP hydrolysis is essential for the substrate to be transported out of the cell.[47] MacA, upon complexing with MacB, is also known to increase the complex's affinity to substrates (i.e., erythromycin)[35]; this enhanced substate affinity might help better prepare MacB in the MacAB-TolC complex for the mechano-transmission step to extrude the bound substrate. Since the presence of ADP has been reported to weaken the MacA-MacB interaction,[22] and the associated change of MacB periplasmic domain significantly affects MacA-TolC assembly,[22] both would lead to the possibility that the complex disassembly is the result of ATP hydrolysis and the release of ADP in step v. Subsequently, in step vi, the released vacant MacB from the disassembled complex is again ready for substrate binding and for MacA to shuttle to another substratebound MacB, which could be facilitated by the geometric proximity from MacB clustering. This mechanism suggests that the excess transporters, preloaded with substrates, drive the limiting adaptor proteins into the formation of a tripartite efflux complex and facilitate substrate translocation by clustering around the functional assembly.

Chemical perturbation supports the functional role of MacB clustering

In the adaptor protein shuttling model, the clustering of excess MacB around the MacAB-TolC complex is important for efficient MacA shuttling (Figure 4). This clustering of MacB could occur via direct MacB dimer interactions with each other or indirect interactions with other IM associated proteins/structures. In *E. coli*, the prokaryotic actin homolog MreB is one of the most important cytoskeleton network proteins located beneath the IM, and it is known that the small molecule A22, i.e., S-(3,4-dichlorobenzyl) isothiourea, can disrupt MreB polymerization,[48,49] which could potentially perturb MacB clustering. Therefore, we treated WT cells with A22 (at 10 μg/mL that is known to reduce cell stiffness immediately and reversibly[50]) and examined the spatial organization of MacB and MacA. For $MacB^{mE}$, the area of its PWDD peak at ~80 nm is halved (Figure 5A), indicating significant $MacB^{mE}$ declustering and supporting that MacB clustering has a contribution from association with cytoskeleton proteins like MreB. In contrast, no substantial perturbation is observed on the PWDD of $MacA^{PmC}$ (Figure 5A), suggesting that the MacAB-TolC complex, where the majority of MacA exists, is not affected by the declustering of MacB.

Based on our functional model (Figure 4), MacB declustering by A22 should hinder efficient MacA shuttling, thus compromising MacAB-TolC efflux function and conferring

less resistance to antibiotics like the macrolide erythromycin. Therefore, we performed a cell erythromycin resistance assay in the presence of A22. We used a Δ*acrAB* deletion strain here so that the ability of MacAB to extrude macrolides is not overshadowed by the efflux complex AcrAB-TolC, a resistance-nodulation-division (RND) family efflux pump that confers broad-spectrum resistance to antibiotics.[9,51] A22 itself has very little effect on cell growth up to 3 μg/mL (Figure S13). With erythromycin alone, cell growth is halved at ~2–3 μg/mL erythromycin (Figure 5B, black). Strikingly, in the presence of A22, cells become more susceptible to erythromycin, and at [A22] = 3 μg/mL, cell growth is almost completely inhibited by 1 μg/mL of erythromycin (Figure 5B), supporting our adaptor protein shuttling model. These results also suggest that antibiotics targeting different cellular processes (i.e., efflux transporter clustering here) can have synergistic, instead of simply additive, functional effects.

Physical perturbation can alter the function of MacAB-TolC

In the adaptor-shuttling mechanism (Figure 4), the assembly of the MacAB-TolC complex is essential for efflux function. Previously, we have shown that physically perturbing the bacterial cell envelope through extrusion loading can disrupt the assembly of a *trans*-envelope metal efflux complex in *E. coli*[52]; we therefore applied extrusion loading here to study MacAB-TolC. This extrusion loading applies mechanical loads via fluid pressure to push and trap individual bacteria inside narrow tapered channels, where the pressure in the microfluidic device is calculated using a hydraulic model (Figure 5C, inset; Note S7; Table S9).[53] At greater pressure differentials (ΔP), the *E. coli* cells travel farther into the channels (Figure S14C), leading to smaller width and smaller surface area (Figures 5C and 5D). Finite element modeling (Note S7; Figures S17 and S18; Tables S10 and S11) shows that octahedral shear stress, which quantifies the distortional stress in the cell envelope, increases with increasing ΔP (Figure 5E), which has been linked previously to increased disassembly of a *trans*-envelope efflux complex.[52]

For both $MacB^{mE}$ and $MacA^{PmC}$ in WT cells under extrusion loading, SMT results show that, with increasing ΔP, the mobile fraction increases (Figure 5F, solid symbols), consistent with mechanical loading-induced disassembly. Interestingly, the diffusion coefficients of their mobile states D_m both decrease (Figure 5G, solid symbols); we attribute this decrease to the reduced cell surface area, which should lead to more crowded membranes and slowed protein motions. No significant changes in $MacB^{mE}$ and $MacA^{PmC}$ clustering were observed, as shown by the clustering peak area from the PWDD analysis (Figure 5H, solid symbols).

Using extrusion loading, we further perturbed the cells and examined $MacB^{mE}$ and $MacA^{PmC}$ behaviors in the presence of A22, which alone can decrease MacB clustering in the cell (Figure 5A). A22 has also been shown to decrease cell stiffness,[53] likely by depolymerizing cytoskeletal MreB filaments that provide circumferential support to the cell.[50] Indeed, A22-treated *E. coli* cells are less stiff, travel farther into the tapered channels (Figure S15), deform to a narrower width, and experience a larger reduction in surface area than non-treated cells with increasing ΔP (Figures 5C and 5D; Table S4). Finite element modeling also shows that A22-treated cells experience a smaller octahedral shear stress

at any ΔP, due to the decrease in material anisotropy of the cell envelope following A22-induced MreB depolymerization (Figure 5E).

Strikingly, in the presence of A22, the mobile fractions of $MacB^{mE}$ and $MacA^{PmC}$ do not increase with increasing ΔP even though more MacAB-TolC disassembly is expected. Instead, the mobile fraction of $MacB^{mE}$ stays almost constant while that of $MacA^{PmC}$ decreases significantly with increasing ΔP (Figure 5F, open symbols). As ΔP-induced complex disassembly was linked with increased octahedral shear stress in the cell envelope, the smaller magnitude of octahedral shear stress in A22-treated cells (Figure 5E) might explain the insignificant change of $MacB^{mE}$'s mobile fraction with increasing ΔP but cannot explain the significant decrease of $MacA^{PmC}$'s mobile fraction. Since A22 alone affects protein clustering in the cell (see earlier), we suspected that there might be significant changes in protein clustering for the A22-treated cells under extrusion loading. Indeed, in the PWDD of $MacB^{mE}$ and $MacA^{PmC}$, the peak at the short distance increases significantly with increasing ΔP for both proteins (Figures 5H, open symbols, S11, and S12), reflecting substantially more protein clustering, which should increase the stationary-state fraction and decreasing the mobile-state fraction. We attribute the increase in clustering in A22-treated cells to the decreased cell stiffness, farther travel into the tapered channels, and a smaller surface area during extrusion loading (Figure 5D). The reduction in surface area would then increase protein density and thereby promote clustering, which is enhanced further as ΔP increases and the surface area decreases further. The significantly reduced diffusion coefficients of the mobile fractions of both MacA and MacB are also consistent with the idea that the membranes are more crowded and protein motion is slowed (Figure 5G).

Altogether, physical perturbation using extrusion loading provides two competing factors in altering *trans*-envelope efflux complex function: octahedral shear stress and cell surface area. Octahedral shear stress impairs complex assembly, while cell surface area affects membrane protein mobility and clustering. Cell stiffness, alterable by A22, plays a significant role in both factors by determining the degree to which octahedral shear stress and cell surface area change, thereby determining the consequence of the mechanical manipulation.

DISCUSSION

By quantifying the cellular concentration and spatiotemporal behaviors of the protein components of the MacAB-TolC multidrug efflux system of the ABC-superfamily in *E. coli*, we revealed the large discrepancy between the cellular protein stoichiometry and the complex assembly stoichiometry as well as the proteins' distinctive localization patterns and diffusive dynamics within different compartments of the cell envelope. These observations led to the proposed adaptor protein shuttling mechanism, which integrates the adaptor protein MacA's dynamic interactions with MacB and TolC, the large excess of MacB transporter, and the dynamic clustering of MacB for efficient sequestration and subsequent efflux of substrates from the periplasm. As multicomponent efflux systems always involve multiple genes that may or may not be encoded in the same operon, and the associated genes differ in length and in their expression efficiencies, we postulate that discrepancy between the cellular protein stoichiometry and the complex assembly stoichiometry is likely

general beyond MacAB-TolC or the ABC superfamily. The large excess of the transporter not only can offer efficient substrate sequestration from the periplasm (e.g., MacB here), but, for other types of transporters, may also provide efflux from the cytosol to the periplasm, where another efflux system can pick up for further extrusion toward the extracellular space. Disproportional protein components are known for other protein assemblies that are not efflux systems,[54] and it is plausible that the excess subunits could have some functional roles as MacB does here. Moreover, dynamic interactions between *trans*-envelope complex components are known for other efflux complexes of different superfamilies[19,20,52] and for other systems such as Lpt machinery[55] and type IV pilus[56]; thus, they are likely broadly relevant as well. Therefore, the adaptor protein shuttling mechanism might apply broadly to multicomponent complexes that traverse the cell envelope of gram-negative bacteria, thus providing general mechanistic insights into such systems in biology. We further showed that chemical and physical factors can perturb different elements of this mechanism, leading to compromised antibiotic resistance of cells. Such combined chemical and physical manipulations may represent innovative synergistic approaches for antimicrobial treatments or at least different approaches to perturb and interrogate their mechanisms.

METHODS

Details regarding the methods can be found in the supplemental methods.

RESOURCE AVAILABILITY

Lead contact—Requests for further information and resources should be directed to and will be fulfilled by the lead contact, Peng Chen (pc252@cornell.edu).

Materials availability—All strains and plasmids generated in this study are available from the lead contact with a completed materials transfer agreement.

Data and code availability

- All data reported in this paper will be shared by the lead contact upon request.
- This paper does not report original code, and all MATLAB codes used in this study have been published previously.[57,58]
- Any additional information required to reanalyze the data reported in this work is available from the lead contact upon request.

Supplementary Material

Refer to Web version on PubMed Central for supplementary material.

ACKNOWLEDGMENTS

This research was supported mainly by NIH grant GM109993 (to P.C.), the mechanobiology component supported by ARO grant W911NF-19–1-0121 (to P.C. and C.J.H), and NSF GRFP DGE-1650441 (to C.E.H.). We thank L.A. Genova and M.F. Roberts for helping with imaging experiments, H. Lin for access to immunoblot imaging instruments, the Cornell Institute of Biotechnology's Imaging Facility with NYSTEM (C029155) and NIH (S10OD018516) funding for the shared Carl Zeiss LSM880 confocal/multiphoton microscope, and the Cornell NanoScale Facility, a member of the National Nanotechnology Coordinated Infrastructure, supported by NSF grant NNCI-2025233.

REFERENCES

1. Viale P, Giannella M, Tedeschi S, and Lewis R (2015). Treatment of MDR-Gram negative infections in the 21st century: a never ending threat for clinicians. Curr. Opin. Pharmacol. 24, 30–37. [PubMed: 26210268]
2. Theuretzbacher U, Outterson K, Engel A, and Karlén A (2020). The global preclinical antibacterial pipeline. Nat. Rev. Microbiol. 18, 275–285. [PubMed: 31745331]
3. Beceiro A, Tomás M, and Bou G (2013). Antimicrobial resistance and virulence: a successful or deleterious association in the bacterial world? Clin. Microbiol. Rev. 26, 185–230. [PubMed: 23554414]
4. Klenotic PA, Moseng MA, Morgan CE, and Yu EW (2021). Structural and Functional Diversity of Resistance-Nodulation-Cell Division Transporters. Chem. Rev. 121, 5378–5416. [PubMed: 33211490]
5. Teelucksingh T, Thompson LK, and Cox G (2020). The Evolutionary Conservation of Escherichia coli Drug Efflux Pumps Supports Physiological Functions. J. Bacteriol. 202, 003677–20.
6. Alav I, Kobylka J, Kuth MS, Pos KM, Picard M, Blair JMA, and Bavro VN (2021). Structure, Assembly, and Function of Tripartite Efflux and Type 1 Secretion Systems in Gram-Negative Bacteria. Chem. Rev. 121, 5479–5596. [PubMed: 33909410]
7. Argüello JM, Raimunda D, and González-Guerrero M (2012). Metal transport across biomembranes: emerging models for a distinct chemistry. J. Biol. Chem. 287, 13510–13517. [PubMed: 22389499]
8. Yum S, Xu Y, Piao S, Sim SH, Kim HM, Jo WS, Kim KJ, Kweon HS, Jeong MH, Jeon H, et al. (2009). Crystal structure of the periplasmic component of a tripartite macrolide-specific efflux pump. J. Mol. Biol. 387, 1286–1297. [PubMed: 19254725]
9. Kobayashi N, Nishino K, and Yamaguchi A (2001). Novel macrolide-specific ABC-type efflux transporter in Escherichia coli. J. Bacteriol. 183, 5639–5644. [PubMed: 11544226]
10. Crow A, Greene NP, Kaplan E, and Koronakis V (2017). Structure and mechanotransmission mechanism of the MacB ABC transporter superfamily. Proc. Natl. Acad. Sci. USA 114, 12572–12577. [PubMed: 29109272]
11. Jo I, Hong S, Lee M, Song S, Kim JS, Mitra AK, Hyun J, Lee K, and Ha NC (2017). Stoichiometry and mechanistic implications of the MacAB-TolC tripartite efflux pump. Biochem. Biophys. Res. Commun. 494, 668–673. [PubMed: 29061301]
12. Fitzpatrick AWP, Llabrés S, Neuberger A, Blaza JN, Bai XC, Okada U, Murakami S, van Veen HW, Zachariae U, Scheres SHW, et al. (2017). Structure of the MacAB-TolC ABC-type tripartite multidrug efflux pump. Nat. Microbiol. 2, 17070. [PubMed: 28504659]
13. Greene NP, Kaplan E, Crow A, and Koronakis V (2018). Antibiotic Resistance Mediated by the MacB ABC Transporter Family: A Structural and Functional Perspective. Front. Microbiol. 9, 950. [PubMed: 29892271]
14. Turlin E, Heuck G, Simões Brandão MI, Szili N, Mellin JR, Lange N, and Wandersman C (2014). Protoporphyrin (PPIX) efflux by the MacAB-TolC pump in Escherichia coli. Microbiologyopen 3, 849–859. [PubMed: 25257218]
15. Yamanaka H, Kobayashi H, Takahashi E, and Okamoto K (2008). MacAB is involved in the secretion of Escherichia coli heat-stable enterotoxin II. J. Bacteriol. 190, 7693–7698. [PubMed: 18805970]
16. Lu S, and Zgurskaya HI (2013). MacA, a periplasmic membrane fusion protein of the macrolide transporter MacAB-TolC, binds lipopolysaccharide core specifically and with high affinity. J. Bacteriol. 195, 4865–4872. [PubMed: 23974027]
17. Tikhonova EB, Devroy VK, Lau SY, and Zgurskaya HI (2007). Reconstitution of the Escherichia coli macrolide transporter: the periplasmic membrane fusion protein MacA stimulates the ATPase activity of MacB. Mol. Microbiol. 63, 895–910. [PubMed: 17214741]
18. Tikhonova EB, and Zgurskaya HI (2004). AcrA, AcrB, and TolC of Escherichia coli Form a Stable Intermembrane Multidrug Efflux Complex. J. Biol. Chem. 279, 32116–32124. [PubMed: 15155734]

19. Santiago AG, Chen TY, Genova LA, Jung W, George Thompson AM, McEvoy MM, and Chen P (2017). Adaptor protein mediates dynamic pump assembly for bacterial metal efflux. Proc. Natl. Acad. Sci. USA 114, 6694–6699. [PubMed: 28607072]
20. Yamamoto K, Tamai R, Yamazaki M, Inaba T, Sowa Y, and Kawagishi I (2016). Substrate-dependent dynamics of the multidrug efflux transporter AcrB of Escherichia coli. Sci. Rep. 6, 21909. [PubMed: 26916090]
21. Tikhonova EB, Dastidar V, Rybenkov VV, and Zgurskaya HI (2009). Kinetic control of TolC recruitment by multidrug efflux complexes. Proc. Natl. Acad. Sci. USA 106, 16416–16421. [PubMed: 19805313]
22. Lu S, and Zgurskaya HI (2012). Role of ATP binding and hydrolysis in assembly of MacAB-TolC macrolide transporter. Mol. Microbiol. 86, 1132–1143. [PubMed: 23057817]
23. Zhang X, Zhang M, Li D, He W, Peng J, Betzig E, and Xu P (2016). Highly photostable, reversibly photoswitchable fluorescent protein with high contrast ratio for live-cell superresolution microscopy. Proc. Natl. Acad. Sci. USA 113, 10364–10369. [PubMed: 27562163]
24. Subach FV, Patterson GH, Manley S, Gillette JM, LippincottSchwartz J, and Verkhusha VV (2009). Photoactivatable mCherry for high-resolution two-color fluorescence microscopy. Nat. Methods 6, 153–159. [PubMed: 19169259]
25. Dammeyer T, and Tinnefeld P (2012). Engineered fluorescent proteins illuminate the bacterial periplasm. Comput. Struct. Biotechnol. J. 3, e201210013. [PubMed: 24688673]
26. Dinh T, and Bernhardt TG (2011). Using superfolder green fluorescent protein for periplasmic protein localization studies. J. Bacteriol. 193, 4984–4987. [PubMed: 21764912]
27. Szczepaniak J, Holmes P, Rajasekar K, Kaminska R, Samsudin F, Inns PG, Rassam P, Khalid S, Murray SM, Redfield C, and Kleanthous C (2020). The lipoprotein Pal stabilises the bacterial outer membrane during constriction by a mobilisation-and-capture mechanism. Nat. Commun. 11, 1305. [PubMed: 32161270]
28. Hendrix J, Flors C, Dedecker P, Hofkens J, and Engelborghs Y (2008). Dark states in monomeric red fluorescent proteins studied by fluorescence correlation and single molecule spectroscopy. Biophys. J. 94, 4103–4113. [PubMed: 18234806]
29. Huang L, Pike D, Sleat DE, Nanda V, and Lobel P (2014). Potential pitfalls and solutions for use of fluorescent fusion proteins to study the lysosome. PLoS One 9, e88893. [PubMed: 24586430]
30. Fu B, Sengupta K, Genova LA, Santiago AG, Jung W, Krzemiński Ł, Chakraborty UK, Zhang W, and Chen P (2020). Metal-induced sensor mobilization turns on affinity to activate regulator for metal detoxification in live bacteria. Proc. Natl. Acad. Sci. USA 117, 13248–13255. [PubMed: 32467170]
31. Kim DH, Park S, Kim DK, Jeong MG, Noh J, Kwon Y, Zhou K, Lee NK, and Ryu SH (2018). Direct visualization of single-molecule membrane protein interactions in living cells. PLoS Biol. 16, e2006660. [PubMed: 30543635]
32. Oswald F, Bank LM, Bollen YJM, and Peterman EJG (2014). Imaging and quantification of trans-membrane protein diffusion in living bacteria. Phys. Chem. Chem. Phys. 16, 12625–12634. [PubMed: 24760126]
33. Chen TY, Jung W, Santiago AG, Yang F, Krzeminski Ł, and Chen P (2015). Quantifying Multistate Cytoplasmic Molecular Diffusion in Bacterial Cells via Inverse Transform of Confined Displacement Distribution. J. Phys. Chem. B 119, 14451–14459. [PubMed: 26491971]
34. Klaus CJS, Raghunathan K, DiBenedetto E, and Kenworthy AK (2016). Analysis of diffusion in curved surfaces and its application to tubular membranes. Mol. Biol. Cell 27, 3937–3946. [PubMed: 27733625]
35. Lin HT, Bavro VN, Barrera NP, Frankish HM, Velamakanni S, van Veen HW, Robinson CV, Borges-Walmsley MI, and Walmsley AR (2009). MacB ABC transporter is a dimer whose ATPase activity and macrolide-binding capacity are regulated by the membrane fusion protein MacA. J. Biol. Chem. 284, 1145–1154. [PubMed: 18955484]
36. Matias VRF, Al-Amoudi A, Dubochet J, and Beveridge TJ (2003). Cryo-transmission electron microscopy of frozen-hydrated sections of Escherichia coli and Pseudomonas aeruginosa. J. Bacteriol. 185, 6112–6118. [PubMed: 14526023]

37. Asmar AT, Ferreira JL, Cohen EJ, Cho SH, Beeby M, Hughes KT, and Collet JF (2017). Communication across the bacterial cell envelope depends on the size of the periplasm. PLoS Biol. 15, e2004303. [PubMed: 29257832]
38. Koronakis V, Sharff A, Koronakis E, Luisi B, and Hughes C (2000). Crystal structure of the bacterial membrane protein TolC central to multidrug efflux and protein export. Nature 405, 914–919. [PubMed: 10879525]
39. Jung W, Sengupta K, Wendel BM, Helmann JD, and Chen P (2020). Biphasic unbinding of a metalloregulator from DNA for transcription (de)repression in Live Bacteria. Nucleic Acids Res. 48, 2199–2208. [PubMed: 32009151]
40. Mullineaux CW, Nenninger A, Ray N, and Robinson C (2006). Diffusion of green fluorescent protein in three cell environments in Escherichia coli. J. Bacteriol. 188, 3442–3448. [PubMed: 16672597]
41. Sochacki KA, Shkel IA, Record MT, and Weisshaar JC (2011). Protein diffusion in the periplasm of *E. coli* under osmotic stress. Biophys. J. 100, 22–31. [PubMed: 21190653]
42. Persson F, Lindén M, Unoson C, and Elf J (2013). Extracting intracellular diffusive states and transition rates from single-molecule tracking data. Nat. Methods 10, 265–269. [PubMed: 23396281]
43. Thomas C, and Tampé R (2020). Structural and Mechanistic Principles of ABC Transporters. Annu. Rev. Biochem. 89, 605–636. [PubMed: 32569521]
44. Rees DC, Johnson E, and Lewinson O (2009). ABC transporters: the power to change. Nat. Rev. Mol. Cell Biol. 10, 218–227. [PubMed: 19234479]
45. Modali SD, and Zgurskaya HI (2011). The periplasmic membrane proximal domain of MacA acts as a switch in stimulation of ATP hydrolysis by MacB transporter. Mol. Microbiol. 81, 937–951. [PubMed: 21696464]
46. Batista Dos Santos W, Souabni H, and Picard M (2023). Corseting a tripartite ABC transporter to make it fit for transport. Biochimie. 205, 117–123. [PubMed: 36442691]
47. Souabni H, Batista Dos Santos W, Cece Q, Catoire LJ, Puvanendran D, Bavro VN, and Picard M (2021). Quantitative real-time analysis of the efflux by the MacAB-TolC tripartite efflux pump clarifies the role of ATP hydrolysis within mechanotransmission mechanism. Commun. Biol. 4, 493. [PubMed: 33888866]
48. Awuni E, and Mu Y (2019). Effect of A22 on the Conformation of Bacterial Actin MreB. Int. J. Mol. Sci. 20, 1304. [PubMed: 30875875]
49. Strahl H, Bürmann F, and Hamoen LW (2014). The actin homologue MreB organizes the bacterial cell membrane. Nat. Commun. 5, 3442. [PubMed: 24603761]
50. Wang S, Arellano-Santoyo H, Combs PA, and Shaevitz JW (2010). Actin-like cytoskeleton filaments contribute to cell mechanics in bacteria. Proc. Natl. Acad. Sci. USA 107, 9182–9185. [PubMed: 20439764]
51. Wang Z, Fan G, Hryc CF, Blaza JN, Serysheva II, Schmid MF, Chiu W, Luisi BF, and Du D (2017). An allosteric transport mechanism for the AcrAB-TolC multidrug efflux pump. Elife 6, e24905. [PubMed: 28355133]
52. Genova LA, Roberts MF, Wong YC, Harper CE, Santiago AG, Fu B, Srivastava A, Jung W, Wang LM, Krzemiński Ł, et al. (2019). Mechanical stress compromises multicomponent efflux complexes in bacteria. Proc. Natl. Acad. Sci. USA 116, 25462–25467. [PubMed: 31772020]
53. Sun X, Weinlandt WD, Patel H, Wu M, and Hernandez CJ (2014). A microfluidic platform for profiling biomechanical properties of bacteria. Lab Chip 14, 2491–2498. [PubMed: 24855656]
54. Taggart JC, Zauber H, Selbach M, Li GW, and McShane E (2020). Keeping the Proportions of Protein Complex Components in Check. Cell Syst. 10, 125–132. [PubMed: 32105631]
55. Lundstedt E, Kahne D, and Ruiz N (2021). Assembly and Maintenance of Lipids at the Bacterial Outer Membrane. Chem. Rev. 121, 5098–5123. [PubMed: 32955879]
56. Kilb A, Burghard-Schrod M, Holtrup S, and Graumann PL (2023). Uptake of environmental DNA in Bacillus subtilis occurs all over the cell surface through a dynamic pilus structure. PLoS Genet. 19, e1010696. [PubMed: 37816065]

57. Chen TY, Santiago AG, Jung W, Krzeminski q., Yang F, Martell DJ, Helmann JD, and Chen P (2015). Concentration- and chromosome-organization-dependent regulator unbinding from DNA for transcription regulation in living cells. Nat. Commun. 6, 7445. [PubMed: 26145755]

58. Chen P, and Chen TY (2020). MATLAB Code Package: iQPALM (Image-based Quantitative Photo-Activated Localization Microscopy) (figshare).

Highlights

- Single-molecule imaging reveals imbalanced stoichiometry of MacAB-TolC components *in vivo*
- Excess MacB shows spatiotemporal behaviors for efficient substrate sequestration and efflux
- The limiting MacA can disassemble from MacAB-TolC and shuttle among clustered MacB
- Chemical or physical perturbation can compromise MacAB-TolC function

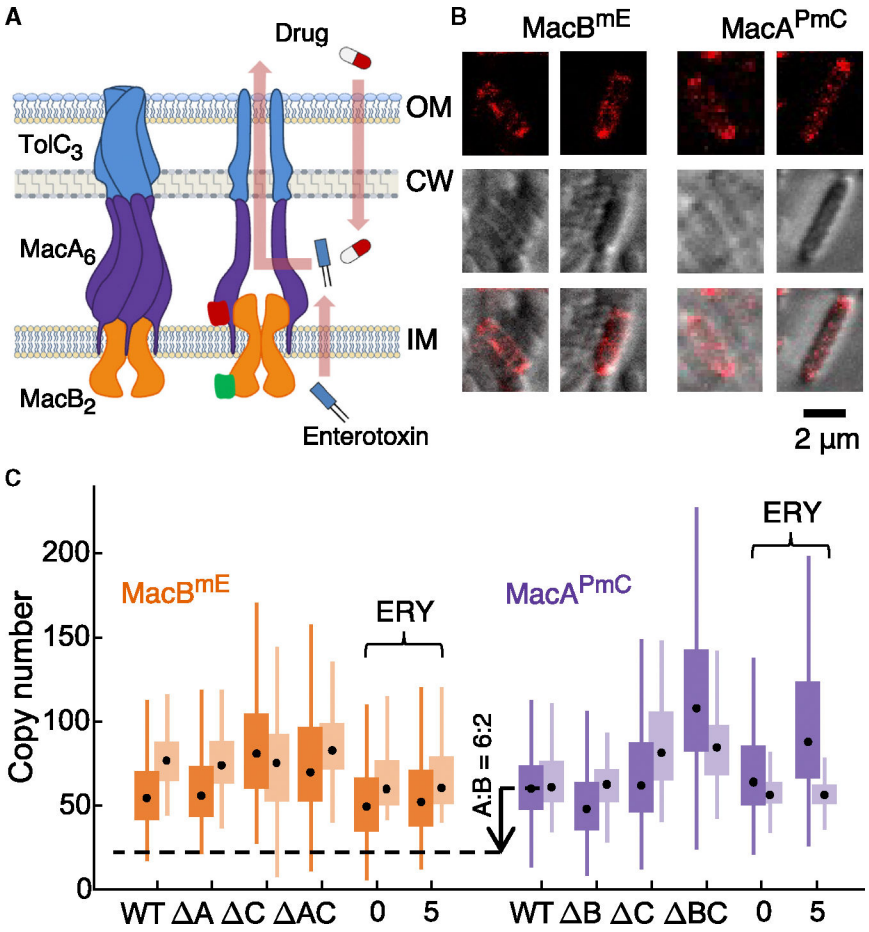

Figure 1. Single-cell protein quantitation reveals the discrepancy between complex and cellular protein stoichiometries of the MacAB-TolC efflux system

(A) Schematic of the assembled MacAB-TolC complex (left) and a sliced view of the complex (right), illustrating $A_6B_2C_3$ stoichiometry, the mEos3.2 tag (green) on MacB, and the PAmCherry1 tag (red) on MacA. CW, cell wall.

(B) Confocal fluorescence images of cells overexpressing $MacB^{mE}$ or $MacA^{PmC}$ (from the top down: a confocal fluorescence image, a transmission image, and a composite image, in which the fluorescence image is overlaid on the transmission image). Note that individual cells show large heterogeneity in protein expression, typical for proteins under plasmid overexpression employed here.

(C) Copy numbers of chromosomally tagged $MacB^{mE}$ or $MacA^{PmC}$ in various strains (n > 300 for each strain) quantified by single-molecule tracking (SMT), followed by single-cell quantification of protein concentration (SCQPC) (darker colors) and whole-cell fluorescence quantitation (lighter colors). Experiments without (0) and with (5 μg/mL) erythromycin (ERY) were conducted on the Δ*acrAB* mutant to increase sensitivity. A dashed horizontal line refers to the expected copy number of MacB on the basis of MacA:MacB = 6:2 stoichiometry in the fully assembled MacAB-TolC complex and of MacA copy number in the WT strain. Dot, median; central box, 25%–75% quantile; length of whisker, 1 times the interquartile range.

See also Figures S4 and S5.

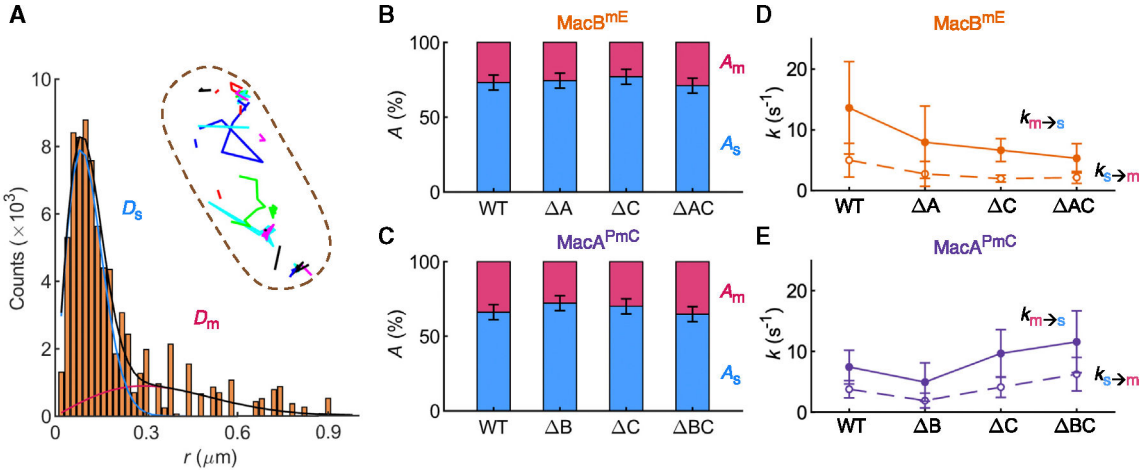

Figure 2. SMT reveals the dynamic behaviors of MacB and MacA in cells

(A) Representative ITCDD-corrected distribution of displacement length r of MacB^{mE} in WT cells (total >38,000 molecules in >3,000 cells). Lines: overall fitting (black) and the resolved mobile (D_m = 0.83 ± 0.05 μm^2·s^{-1}, red) and quasi-stationary (D_s = 0.055 ± 0.002 μm^2·s^{-1}, blue) diffusion states. Inset: overlay of tracking trajectories of MacB^{mE} molecules in a single WT cell. Brown dashed line, cell contour.

(B and C) Fractional populations of the mobile (A_m, red) and quasi-stationary (A_s, blue) diffusion states of MacB^{mE} (B) and MacA^{PmC} (C) in various strains. The D and A values of all strains are summarized in Tables S5 and S6.

(D and E) Effective interconversion rate constants between the mobile and quasi-stationary states, $k_{m\rightarrow s}$ and $k_{s\rightarrow m}$, of entering and leaving the quasi-stationary state, respectively, for MacB^{mE} (D) and MacA^{PmC} (E).

Error bars in (B)−(E): SD.

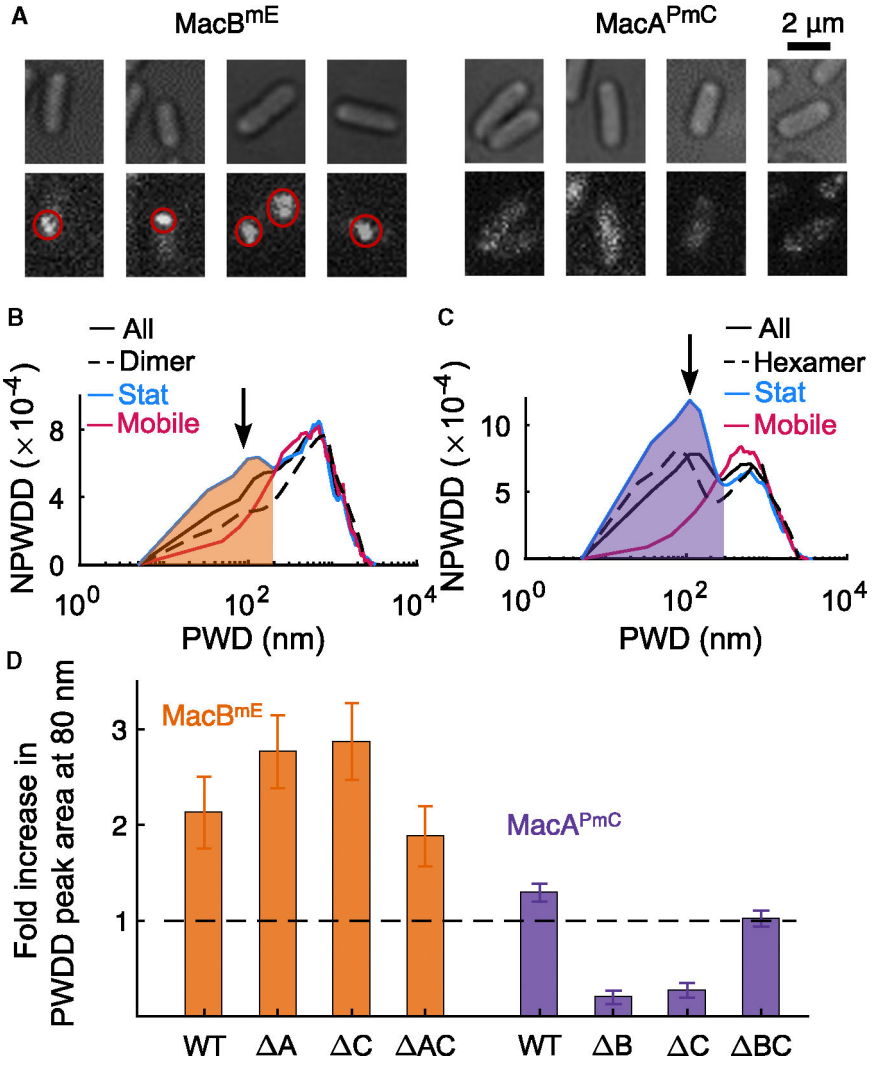

Figure 3. Distinct spatial organization patterns of MacB^{mE} and MacA^{PmC} in the cell

(A) Transmission (top) and wide-field fluorescence (bottom) images of MacB^{mE} or MacA^{PmC} in WT strains in which all mE/PmC are photoactivated; the granular features of MacB^{mE} are circled in red.

(B and C) Normalized PWDD (i.e., NPWDD) of first locations of MacB^{mE} (B) and MacA^{PmC} (C) in WT strains. Black lines, all MacB^{mE}/MacA^{PmC} molecules; red, mobile molecules; blue, quasi-stationary molecules; black dashed line, from simulations of randomly localized dimers or hexamers on the cell membrane. The PWDD peak of quasi-stationary molecules at the short distance of ~80 nm is shaded and denoted by black arrows, whose area reflects the extent of clustering and/or oligomerization.

(D) Fold increase of PWDD peak area at 80 nm to the simulated PWDD peak area of random distribution at 80 nm of MacB^{mE} and MacA^{PmC} in various strains. Black dashed line, simulations of randomly located dimers (for MacB^{mE}) or hexamers (for MacA^{PmC}). Error bars: SD.

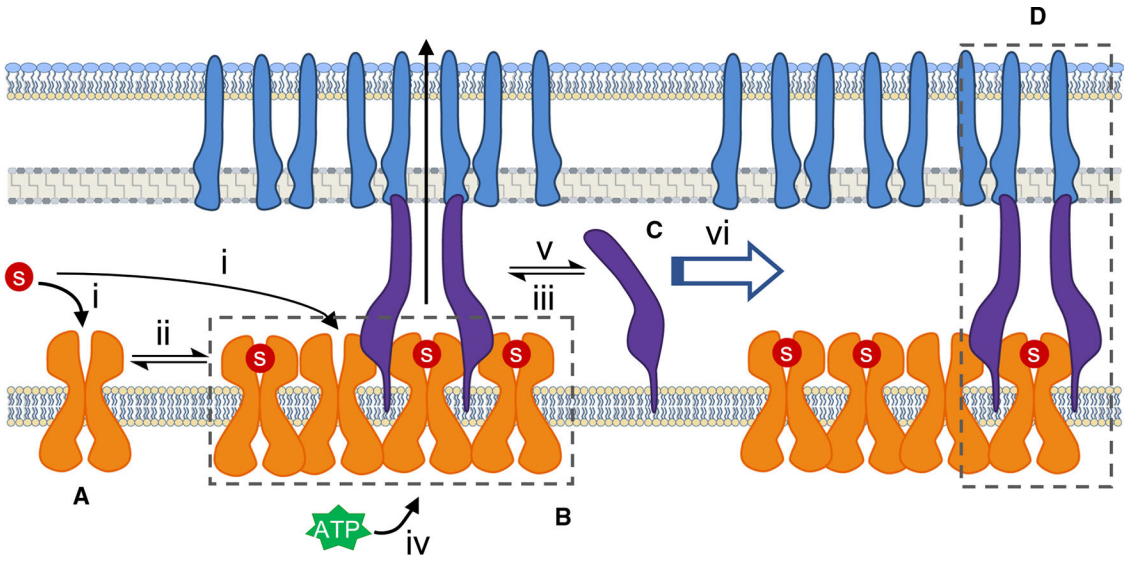

Figure 4. Adaptor protein shuttling model for MacAB-TolC efflux in the presence of transporter excess and clustering

(A) Unassembled, freely moving $MacB_2$ dimers.

(B) Clustered $MacB_2$ dimers.

(C) Unassembled, mobile MacA.

(D) Fully assembled MacAB-TolC complex.

A sequence of steps is involved. (i) Substrates (red) bind to vacant, uncomplexed MacB (orange) from the periplasm side. (ii) The substrate-bound MacB dynamically clusters around the assembled complex. (iii) MacA (purple) shuttles over to the substrate-bound MacB, together with the abundant OM TolC (blue), to form the MacAB-TolC complex. (iv) ATP is recruited to extrude the substrate by mechano-transmission. (v) MacAB-TolC disassembles with the release of ADP and Pi. (vi) MacA shuttles to another nearby substrate-bound MacB, repeating step iii, and the vacant MacB is ready to capture substrates from the periplasm, repeating step i.

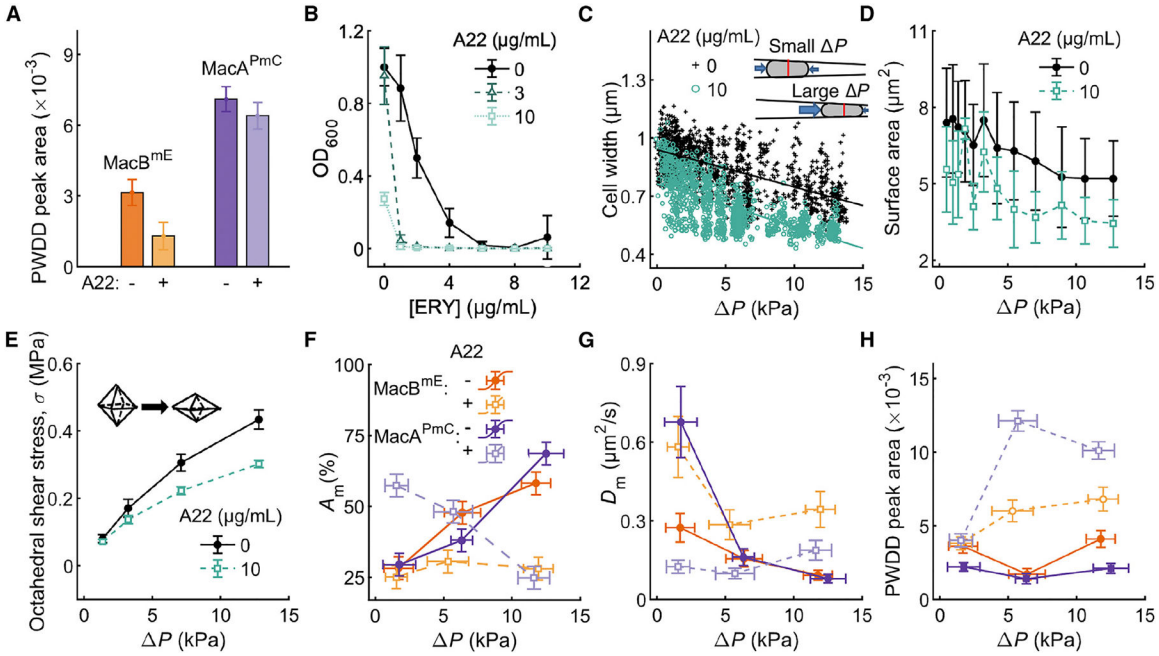

Figure 5. Chemical and physical perturbations of MacAB-TolC function

(A) Area of normalized PWDD peak at ~80 nm for $MacB^{mE}$ and $MacA^{PmC}$ in cells without or with 10 μg/mL A22 treatment.

(B) 22 h cell culture optical density 600 vs. [ERY] in the absence or presence of different concentrations of A22.

(C) Deformed cell width of individual cells during extrusion loading vs. ΔP for cells without (n = 1,363) and with (n = 1,317) 10 μg/mL A22 treatment. Lines: linear fits. Inset: Schematic of ΔP-induced cell deformation in extrusion loading.

(D) Cell surface area vs. ΔP for cells without (n = 306) or with (n = 897) 10 μg/mL A22 treatment.

(E) Finite element analysis-derived octahedral shear stress in the cell envelope vs. ΔP (inset). Shown is a representation of octahedral shear stress on an infinitesimally small segment of the cell envelope. The segment volume is constant, but the shape is deformed.

(F–H) Fractional populations of the mobile state (A_m). (F), diffusion coefficients of the mobile state (D_m) (G), and area of normalized PWDD peak at ~80 nm (H) vs. ΔP for $MacB^{mE}$ and $MacA^{PmC}$ in cells without and with 10 μg/mL A22 treatment. For $MacB^{mE}$, n = 584 and 627 cells, respectively. For $MacA^{PmC}$, n = 512 and 566 cells, respectively. The distribution of ΔP experienced by cells is shown in Figure S16. The legend in (F) applies to (F) and (G).

Error bars in (A), (B), and (D)–(H) are SD.